*Supplementary information for RSC Advances*

# Study on fracture behaviour of individual InAs nanowires using an electron-beam-drilled notch

Suji Choi,[‡ab] Jong Hoon Lee,[‡a] Min Wook Pin,[ac] Dong Won Jang,[d] Seong-Gu Hong,[a] Sang Jun Lee,[a] Jong Seok Jeong,[e] Seong-Hoon Yi,*[b] and Young Heon Kim*[ac]

[a]Korea Research Institute of Standards and Science, 267 Gajeong-Ro, Yuseong-Gu, Daejeon 34113, Republic of Korea.

[b]Department of Materials Science and Metallurgical Engineering, Kyungpook National University, Daegu 41566, Republic of Korea.

[c]University of Science & Technology, 217 Gajeong-Ro, Yuseong-Gu, Daejeon 34113, Republic of Korea.

[d]School of Mechanical, Aerospace and Systems Engineering, Korea Advanced Institute of Science and Technology, Daejeon 34141, Republic of Korea.

[e]Department of Chemical Engineering and Materials Science, University of Minnesota, Minneapolis, Minnesota 55455, United States.

‡ These two authors contributed equally to this work and are co-first authors.

* Corresponding author: young.h.kim@kriss.re.kr; yish@knu.ac.kr

**Table S1.** Mechanical properties of InAs nanowires reported by various research groups. Elastic modulus, $E$, Fracture tensile strain, $\varepsilon$, and fracture strength, $\sigma_f$, are denoted.

| No. | Technique | Synthetic method | Structure | $\sigma_f$ (GPa) | $\varepsilon$ (%) | $E$ (GPa) | Size dependence |
|---|---|---|---|---|---|---|---|
| 1 | Stroboscope[1] | CBE | ZB+WZ | - | - | 40-100 | O |
| 2 | Nanomanipulators [2] | MOCVD | ZB+WZ | 1.9-4.4 | 4.1-11.2 | 16-78 (avg. 45) | × |
| | | MBE | WZ | 2.5-4.8 | 5.2-9.7 | 34-79 (avg. 58) | × |
| 3 | Atomic force microscope[3] | MBE | WZ | - | - | 43.5 | - |

**Table S2.** Diameters, elastic modulus, fracture strains, and fracture strengths for all 20 InAs NWs measured in our experiments.

| No. | Diameter (nm) | Elastic modulus (GPa) | Strain (%) | Stress (GPa) |
|---|---|---|---|---|
| 1 | 120.1 | 78.4 | 7.1 | 5.6 |
| 2 | 59.4 | 78.4 | 6.3 | 4.9 |
| 3 | 100 | 65.5 | 5.9 | 3.9 |
| 4 | 96.7 | 82.1 | 4.8 | 3.9 |
| 5 | 94.6 | 74.14 | 7.4 | 5.5 |
| 6 | 87 | 83.8 | 5.5 | 4.6 |
| 7 | 103 | 91.9 | 3.7 | 3.4 |
| 8 | 57.3 | 56 | 6.5 | 3.6 |
| 9 | 101.8 | 54.7 | 6.1 | 3.3 |
| 10 | 73.7 | 56.9 | 5.2 | 2.9 |
| 11 | 71.9 | 50.7 | 5.9 | 3.0 |
| 12 | 86.2 | 91 | 5.6 | 5.1 |
| 13 | 92.1 | 65.2 | 6.2 | 4.0 |
| 14 | 86.6 | 72.1 | 6.7 | 4.8 |
| 15 | 87.3 | 73 | 6.2 | 4.5 |
| 16 | 84.9 | 74 | 6.1 | 4.5 |
| 17 | 74 | 91.8 | 5.6 | 5.2 |
| 18 | 74 | 83.2 | 4.7 | 3.9 |
| 19 | 98.8 | 70.8 | 4.3 | 3.1 |
| 20 | 114 | 45.7 | 4.2 | 1.9 |
| Avg. | 88.2 | 72.0 | 5.7 | 4.1 |

**Supplementary Information S1: Transfer procedure of a single InAs NW on the PTP device**

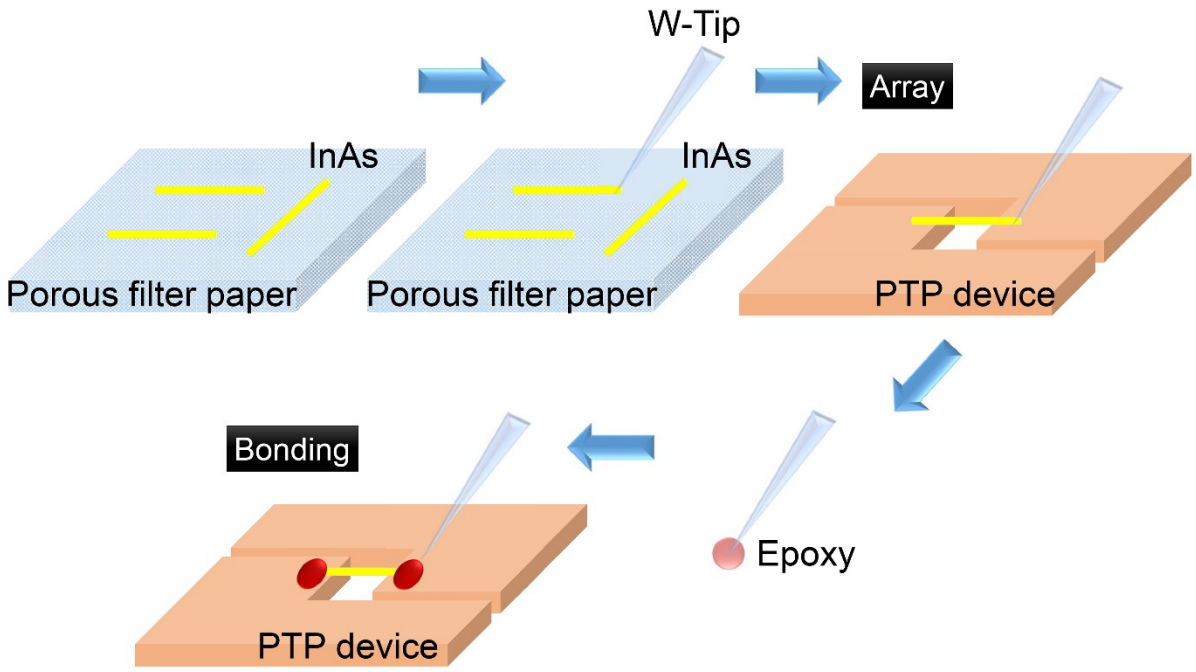


**Figure S1.** Schematic illustration for the transfer of the InAs NW from the substrate to the PTP device. A single InAs NW on the porous filter paper was attached to a tungsten (W) tip and moved onto the PTP devices. A small amount of viscous epoxy was applied using a W- tip to fix the edges of the InAs NW to the PTP device. The epoxy was cured at room temperature. The proper application of the epoxy was confirmed by scanning electron microscope.

## Supplementary Information S2: Real-time TEM observation during the tensile testing

: Figures S2a and S2b show the TEM images captured before and after the fracture, respectively (from Supporting Information V1). The mechanical fracture of the InAs NW occurs at the region where stress is concentrated, although the distribution of stress is relatively uniform throughout the NW before the fracture. The magnified TEM image in Figure S2c shows the end of the remaining part of the InAs NW after the fracture. Figures S2d and S2e show the discontinuous changes in the atomic structures in the NWs that we observed (indicated by dotted lines). We also detected a locally amorphous-like atomic structure (only several nanometers in length) with the HRTEM image (the dashed circle in Figure 2e).

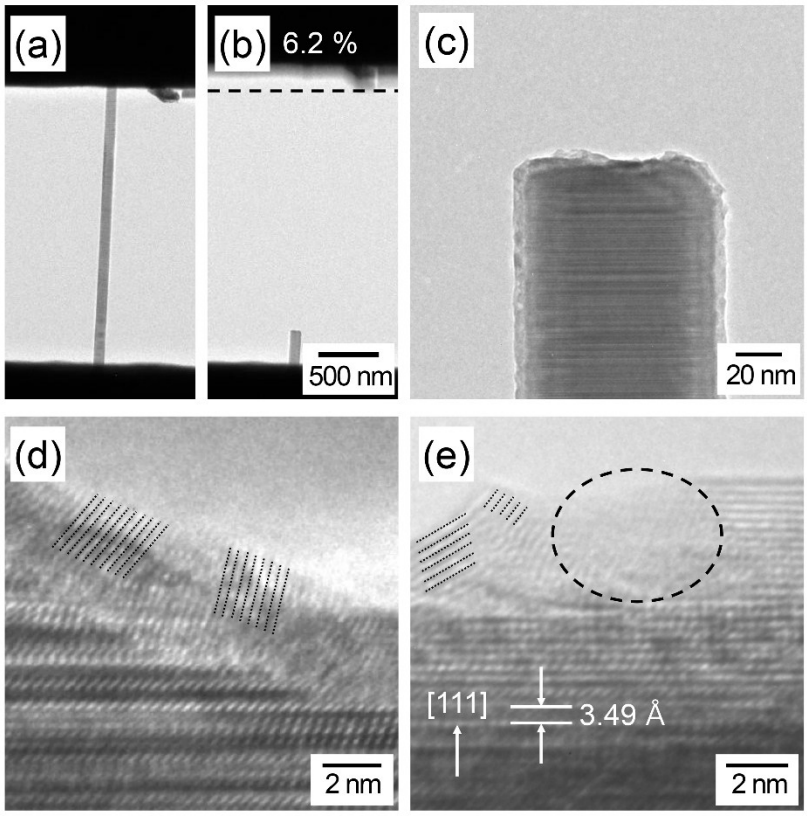


**Figure S2.** (a-b) BFTEM images of a InAs NW without notches before and after fracturing during the tensile test. The fracture strain is indicated in (b). (c) Magnified TEM image at the fracture location after the tensile test. (d-e) HRTEM images taken near the fracture surface. A discontinuity of lattice planes was observed near the fracture surface; the dotted lines show the deformation of the atomic structures after the fracture.

## Supplementary Information S3: Calculation of cohesive energy per In-As pair

The first principle calculations for the total energy of InAs were performed within the the density functional theory (DFT) framework within the local-density approximation (LDAs) and generalized gradient approximation (GGA), as implemented in the Cambridge Serial Total Energy Package (CASTEP).[4–9] Ultrasoft type pseudopotentials and the exchange-correlation function based on LDA-CAPZ and GGA-PBE were adopted for the calculations. The Brillouin zone was sampled with the Monkhorst-Pack scheme using a k point 6 x 6 x 6 mesh.[10] A plane-wave energy cutoff of 450 eV and an energy convergence limit of $1\times10^{-7}$ eV/atom were used for the total energy calculations, thus guaranteeing a high level of convergence. The geometry of the resulting structures was fully optimized using the 3 Broyden-Fletcher-Goldfarb-Shanno (BFGS) minimization technique with the following tolerances: residual force less than 0.01 eV/Å, and residual bulk stress less than 0.02 GPa.

Using the calculation procedure stated above, the total energies for InAs, $E_{tot,\ solid}$, were obtained. The cohesive energies were obtained as $E_{coh} = E_{tot,\ solid} - \Sigma_i E_{atom,i}$ per unit cell. The cohesive energy per unit cell, $E_{coh}$, was then divided by four to seek the cohesive energy per In-As pair, $E_{coh,\ In\text{-}As}$, because four indium (In) and four arsenic (As) atoms are included in the unit cell.

| Exchange-correlation function | Cohesive energy per In-As pair (eV) |
|---|---|
| LDA-CAPZ | 9.07 |
| GGA-PBE | 7.71 |

*This value is similar to that reported by Panse et al.[11]

## Supplementary Information S4: Electron-beam drilling process

By applying the FEB, it is possible to remove a material from the specimen by controlling direct atomic displacement by inelastic collision and ionization (or excitation). An incident electron beam transfers a significant amount of energy to the atoms of the specimen by a direct collision, which can be sufficient to sputter it from the surface.[12–14] The maximum energy ($E_{max}$) that can be transferred to an atom in a collision is:[15,16]

$$E_{max} = \frac{2E\left(E + 2m_0c^2\right)}{M_0c^2} \tag{1}$$

where $E$ is the energy of incident electrons, $M_0$ is the mass of the atom, and $m_0c^2$ (= 511 eV) is the rest energy of the electron. From equation (1), the maximum transfer energies for In and As, $E_{max,\ In}$ and $E_{max,\ As}$, are approximated to 7.42 and 11.37 eV at 300 keV, respectively. The displacement cross section for sputtering, $\sigma_d$, the probability that an electron displaces the target atom, is given as follows:[17,18]

$$\sigma_d = \pi\left(\frac{Ze^2}{m_0C^2}\right)^2\frac{1-\beta^2}{\beta^4}\left[(\xi-1) - \beta^2\ln(\xi) + \pi\alpha\beta\left\{2\left(\xi^{\frac{1}{2}} - 1\right) - \ln(\xi)\right\}\right], \tag{2}$$

where $\alpha = Z/137$, $\beta$ is a relativistic correction factor, $\beta = v/c = \sqrt{1-(1+\frac{E}{mc^2})^{-2}}$, and $\xi = E_{max}/E_d$.

To calculate the $\sigma_d$, it is necessary to determine the displacement energy, $E_d$, of InAs. For the calculation of the cross-section, the cohesive energy, $E_{coh,\ In\text{-}As}$, was adopted as the displacement energy, $E_d$. Because each In atom has four As neighbors in a ZB InAs crystal and the number of bonds ($N$) can be changed from one to four during the displacement process, various cohesive energies depending on the number of bonds were chosen for the calculation.[19] And the total-energy and force calculations for $E_{coh,\ In\text{-}As\ pair}$, the cohesive energy per In-As pair considered as the maximum displacement energy, were performed using the framework of the

density functional theory (DFT; see Supplementary Information S3).[11] Since, the value of $E_d$ in the range of 1.55–9.07 eV was used for the calculation of the cross section for sputtering.

The cross section of radiolytic movement of atoms in a specimen is related with the ionization or excitation of electrons by inelastic scattering. The cross section of radiolytic movement by inelastic scattering is shown by equation (3): [15–17]

$$\sigma_{in} = \frac{8\pi a_0^2 E_R^2}{m_0 c^2} \frac{Z}{E_{th}\beta^2} \times \zeta, \tag{3}$$

where $a_0$ is the Bohr radius (5.29 × $10^{-11}$ m), $E_R$ is the Rydberg energy for hydrogen ( $E_R = \frac{m_0 e^4}{2\hbar^2} = 13.606\ eV$), $E_{th}$ is the threshold energy that must be transferred to the electrons of the solid to produce atomic movement, and the experimental efficiency factor, $\zeta$. The threshold energy, $E_{th}$, of 6.20 eV was selected for the calculation of the $\sigma_{in}$ [cohesive energy per In-As bond = 1.55 eV, coordination number = 4], because the $E_{th}$ is decided by the bond strength and the coordination number of the atom. And, the efficiency factor $\zeta$ in the range of ~$10^{-3}$ to ~$10^{-5}$ was used for the calculation. The cross section of radiolytic movement by inelastic scattering for InAs, $\sigma_{in,\ InAs}$, calculated based on equation (3) as a function of the incident electron energy.

## Supplementary Information S5: Dependence of the electron beam drilling on the kinetic energy of the electrons and the current density

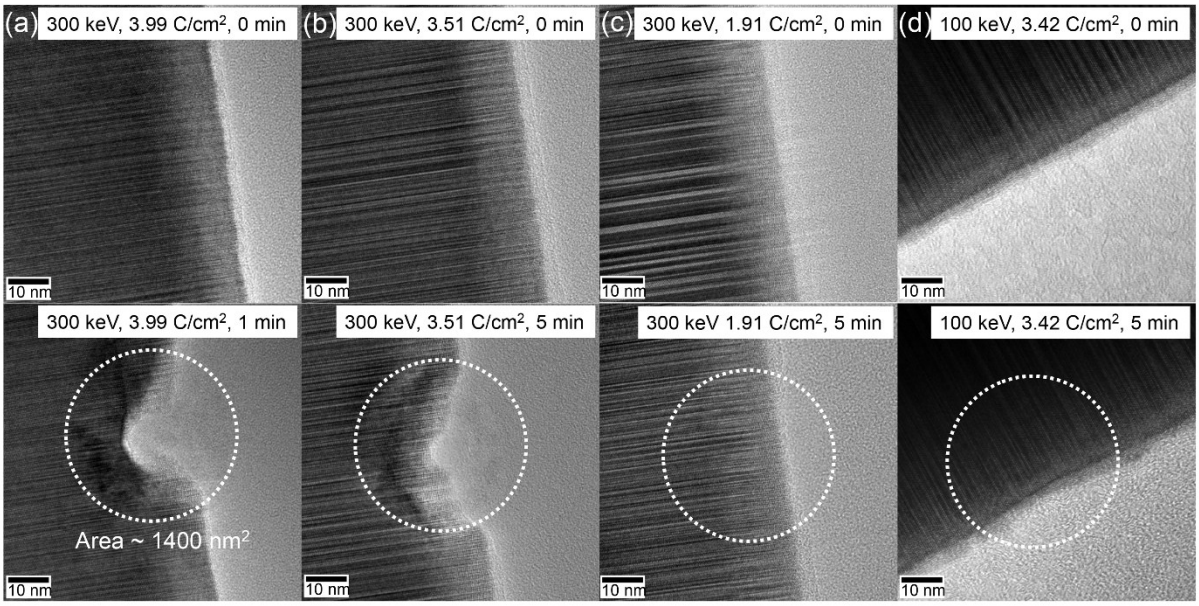


**Figure S3.** Dependence on the kinetic energy of electrons and the current density of the drilling. (a) 300 keV, 3.99 C/cm$^2$, 1 min. (b) 300 keV, 3.51 C/cm$^2$, 5 min. (c) 300 keV, 1.91 C/cm$^2$, 5 min. (a) 300 keV, 3.42 C/cm$^2$, 5 min. At the lower current density and kinetic energy, the electron beam drilling was weak ((c) and (d)).

**Supplementary Information S6: A schematic diagram of notches formed on InAs NWs**

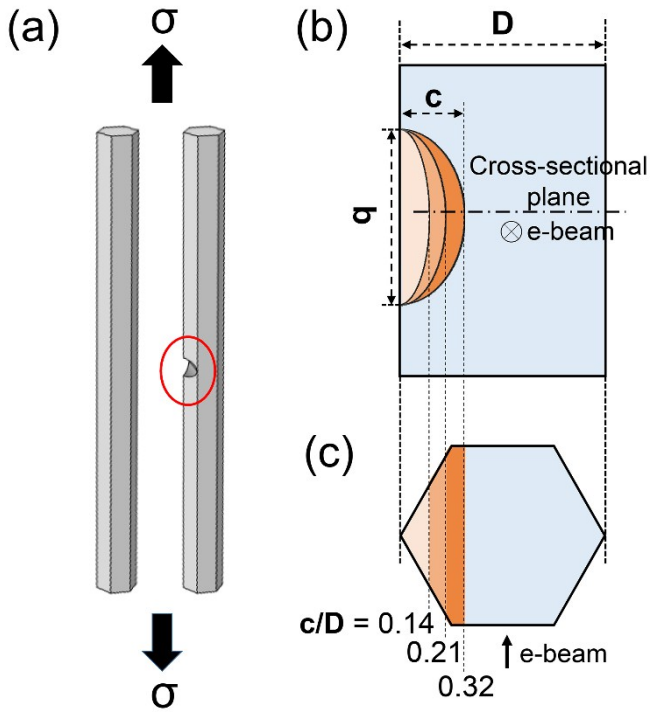


**Figure S4.** (a) A schematic diagram of InAs NWs without (left) and with (right) notches. (b) Detail of the notch shape. The width, b, was fixed, while the depth, c, was controlled to evaluate fracture toughness. Supposed cross-sectional shape of the InAs NWs (bottom). (c) The relative notch size was defined to c/D, where D is the NW diameter.

**Supplementary Information S7: Graphical visualization of stress concentration on the InAs NWs with a notch**

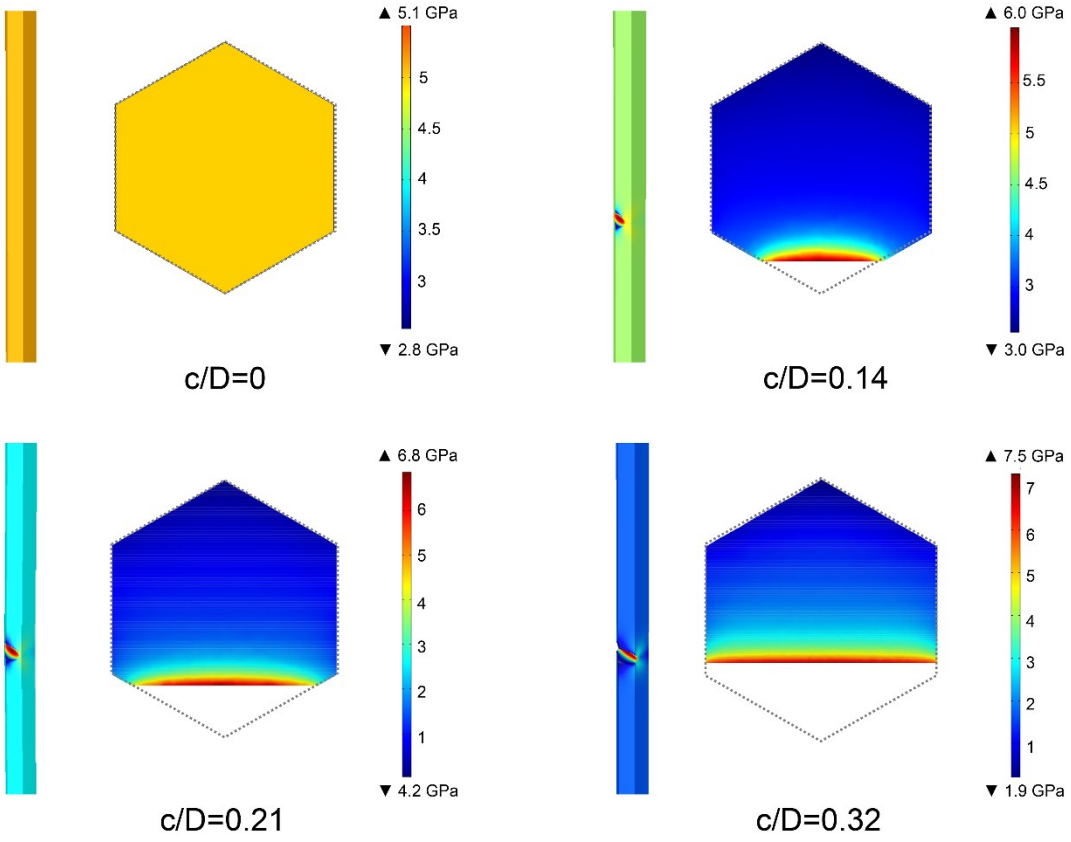


**Figure S5.** (a-d) Graphical stress distributions via FEM simulation on the individual InAs NWs with relative notch sizes 0%, 14%, 21%, and 32%, respectively. The stress is concentrated at the center of the notch.

## References


1 M. Lexholm, I. Karlsson, F. Boxberg and D. Hessman, *Appl. Phys. Lett.*, 2009, **95**, 113103.
2 X. Li, X. L. Wei, T. T. Xu, Z. Y. Ning, J. P. Shu, X. Y. Wang, D. Pan, J. H. Zhao, T. Yang and Q. Chen, *Appl. Phys. Lett.*, 2014, **104**, 103110.
3 R. Erdélyi, M. Hannibal Madsen, G. Sáfrán, Z. Hajnal, I. Endre Lukács, G. Fülöp, S. Csonka, J. Nygård and J. Volk, *Solid State Commun.*, 2012, **152**, 1829–1833.
4 P. Hohenberg and W. Kohn, *Phys. Rev.*, 1964, **136**, B864–B871.
5 W. Kohn and L. J. Sham, *Phys. Rev.*, 1965, **140**, A1133–A1138.
6 J. P. Perdew and W. Yue, *Phys. Rev. B*, 1986, **33**, 8800–8802.
7 J. P. Perdew, K. Burke and M. Ernzerhof, *Phys. Rev. Lett.*, 1996, **77**, 3865–3868.
8 M. D. Segall, P. J. D. Lindan, M. J. Probert, C. J. Pickard, P. J. Hasnip, S. J. Clark and M. C. Payne, *J. Phys. Condens. Matter*, 2002, **14**, 2717.
9 S. J. Clark, M. D. Segall, C. J. Pickard, P. J. Hasnip, M. I. J. Probert, K. Refson and M. C. Payne, *Z. Für Krist. - Cryst. Mater.*, 2009, **220**, 567–570.
10 H. J. Monkhorst and J. D. Pack, *Phys. Rev. B*, 1976, **13**, 5188–5192.
11 C. Panse, D. Kriegner and F. Bechstedt, *Phys. Rev. B*, 2011, **84**, 75217.
12 D. L. Medlin and D. G. Howitt, *Philos. Mag. Lett.*, 1991, **64**, 133–141.
13 D. A. Muller and J. Silcox, *Philos. Mag. A*, 1995, **71**, 1375–1387.
14 K. A. Mkhoyan and J. Silcox, *Appl. Phys. Lett.*, 2003, **82**, 859–861.
15 R. Csencsits and R. Gronsky, *Ultramicroscopy*, 1987, **23**, 421–431.
16 O. Ugurlu, J. Haus, A. A. Gunawan, M. G. Thomas, S. Maheshwari, M. Tsapatsis and K. A. Mkhoyan, *Phys. Rev. B*, 2011, **83**, 113408.
17 L. W. Hobbs, in *Introduction to Analytical Electron Microscopy*, eds. J. J. Hren, J. I. Goldstein and D. C. Joy, Springer US, 1979, pp. 437–480.
18 H.-M. Kim, M.-H. Lee and K.-B. Kim, *Nanotechnology*, 2011, **22**, 275303.
19 W. A. Harrison, *Electronic Structure and the Properties of Solids: The Physics of the Chemical Bond*, Dover: New York, 1989.